THE JOURNAL OF PHYSICAL CHEMISTRY LETTERS
A JOURNAL OF THE AMERICAN CHEMICAL SOCIETY

pubs.acs.org/JPCL

Letter

Ultrafast Self-Assembly of Colloidal Photonic Crystals during Low-Pressure-Assisted Evaporation of Droplets

Chen Zhang, Weibin Li,* and Yuren Wang*

Cite This: *J. Phys. Chem. Lett.* 2022, 13, 3776−3780

Read Online

ACCESS | Metrics & More | Article Recommendations | Supporting Information

ABSTRACT: After evaporation of a sessile colloidal droplet, the coffee stain always emerges with disordered structures. This may be unfavorable for many applications, such as droplet-based printing. Therefore, to realize uniform and ordered patterns is becoming an urgent task. In this work, we realize ultrafast fabrication of uniform colloidal crystals by suppressing the coffee ring effect in flash evaporation of a droplet. The low-pressure environment can tremendously improve the evaporation rate, which will accelerate the colloidal particles to be captured by the gas−liquid interface and self-assemble into ordered structures instantaneously. With the control of the pressure and concentration, the uniform and ordered patterns can be realized in several seconds. The colloidal photonic crystals with diverse structural colors can be easily and rapidly obtained by adjusting the particle sizes. We think this work may have instructive significance in the rapid fabrication of high-quality and high-performance printed electronics.

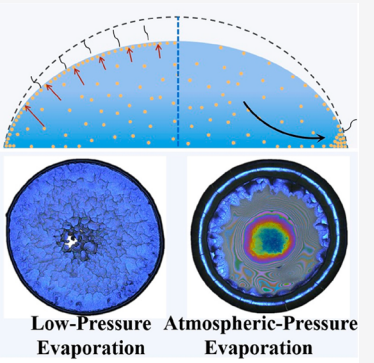

Evaporation of colloidal droplets has attracted increasing attention,[1−3] not only because rich and diverse physical phenomena emerge, including the coffee ring effect, but also its widespread applications in industry,[4,5] such as printing and coating technologies,[6,7] medical diagnosis,[8] and biochemical detection.[9] To achieve a uniform and ordered pattern is becoming quite necessary for many potential applications, such as printed electronics,[10,11] because the high-quality printed structures are the foundation of high-performance devices.[12]

The pattern formation from an evaporating droplet is closely related to its evaporation processes. Therefore, a large number of studies focus on evaporative convection and particle transport, to control the morphology and structure of the deposition patterns.[13−15] It mainly involves the capillary flow and the Marangoni flow inside the droplet. The capillary flow, which is caused by the uneven evaporation flux, can transport colloidal particles toward the edge of the droplet and form a coffee ring structure.[16] Then, the structure can present a transition from ordered arrays to disordered packing.[17] The Marangoni flow, which results from the surface tension gradient,[18,19] may be caused by the temperature gradient, solvent concentration gradient, or surfactants. The Marangoni recirculating flow has complex influences on the deposition pattern.[20] Besides, the deposition pattern can be affected by the Derjaguin−Landau−Verwey−Overbeek (DLVO) attraction between the particles and the substrate,[21] the sedimentation effect of gravity,[22,23] and the interfacial capture effect.[24] Therefore, the comprehensive effects of these complex convections and dynamic processes determine the morphology of the final deposition patterns. Although a lot of work has been conducted to suppress the coffee ring and obtain uniform patterns by regulating the Marangoni effect,[25] wettability of substrate,[26] acoustic fields,[27] and particle shapes,[28] the disordered microstructures and a large number of defects are inevitable for these patterns.

Evaporation-driven self-assembly on the gas−liquid interface has been proven to be a simple and low-cost way of constructing long-range ordered structures.[29] However, the slow evaporation rate will lead to low assembly efficiency. Although Li et al. have realized the rapid assembly of particles in water-based colloidal droplets by heating methods,[30] the high temperature can easily result in complex convections, such as the thermal Marangoni flow and the Rayleigh−Benard flow. These extra flows are not conducive to the formation of ordered structures. For example, the Marangoni flow could easily result in defects of the printed film.[31] In comparison to heating the substrate, we assume that the low-pressure-assisted evaporation (LPAE) may not cause extra internal flow; therefore, the microstructure of the deposits could be more uniform. In addition, LPAE is more appropriate to temperature-sensitive polymer substrates or biological samples than heating methods. In this letter, we study the rapid evaporation dynamics of colloidal droplets by the LPAE method, further revealing the mechanisms of ultrafast assembly behavior on the gas−liquid interface, and finally realize the regulation and

Received: February 22, 2022
Accepted: April 14, 2022
Published: April 21, 2022

https://doi.org/10.1021/acs.jpclett.2c00534
J. Phys. Chem. Lett. 2022, 13, 3776−3780

construction of the ordered structure of colloidal photonic crystals.

Aqueous colloidal droplets dispersed with polystyrene microspheres were gently deposited on a hydrophilic glass substrate. Then, the glass substrate was put into a vacuum tank, whose pressure can be adjusted, as shown in Figure S1 of the Supporting Information. The real-time evolution process of the droplets was recorded by the microscope with diverse pressures. The structures of the final patterns were characterized by the spectrometer and scanning electron microscope (see part 1 of the Supporting Information for details). Experimental results show that colloidal droplets can evaporate completely in a few seconds under the LPAE. Correspondingly, atmospheric pressure evaporation takes several minutes.

The fast evaporation of the droplet can be described by the quasi-steady-state evaporation theory. The steam around the droplet is assumed as an ideal gas, and the droplet evaporates as a constant contact radius (CCR) mode. Then, the mass change rate $\dot{m}$ in the process of evaporation satisfies[32]

$$-\dot{m} = \pi RDC_v(1 - H)(0.27\theta^2 + 1.3) \quad (1)$$

where $R = 0.91 \times 10^{-3}$ m is the droplet radius, $C_v = 1.63 \times 10^{-2}$ kg/m^3 is the saturated vapor concentration, $H = 0.22$ is the water content, θ is the contact angle between the droplet and the substrate varying with time, $\theta_0 = 38°$ is the initial contact angle, $T = 292$ K is the ambient temperature of the experiment, and $\rho = 1000$ kg/m^3 is the density of water. The vapor diffusion coefficient D is related to the pressure, which satisfies

$$D = D_0 \frac{P_0}{P}\left(\frac{T}{T_0}\right)^{3/2} \quad (2)$$

where $D_0 = 0.22 \times 10^{-4}$ m^2/s is the diffusion coefficient of water vapor under standard conditions and $T_0 = 273$ K. The final evaporation time t_s of a sessile spherical cap droplet satisfies[33]

$$\int_0^{t_s} (\dot{m})\mathrm{d}t = m \quad (3)$$

where

$$m = \frac{\frac{\pi}{3}R^3(1 - \cos\theta_0)^2(2 + \cos\theta_0)\rho}{(\sin\theta_0)^3} \quad (4)$$

We consider that $\theta(t)$ varies linearly with time;[32] therefore, we can assume

$$\theta(t) = -\frac{\theta_0}{t_s}t + \theta_0 \quad (5)$$

then

$$\int_0^{t_s}\left(0.27\left(1 - \frac{t}{t_s}\right)^2\theta_0^2 + 1.3\right)\mathrm{d}t = \frac{m}{\pi RDC_v(1 - H)} \quad (6)$$

Therefore, the relationship between evaporation time (t_s) and pressure (P) can be deduced from eqs 1−6.

$$t_s = 356\frac{P}{P_0} \quad (s) \quad (7)$$

From eq 7, we can find that the evaporation time is proportional to pressure. This theoretical relationship can be represented by the solid line in Figure 1b. The discrete points

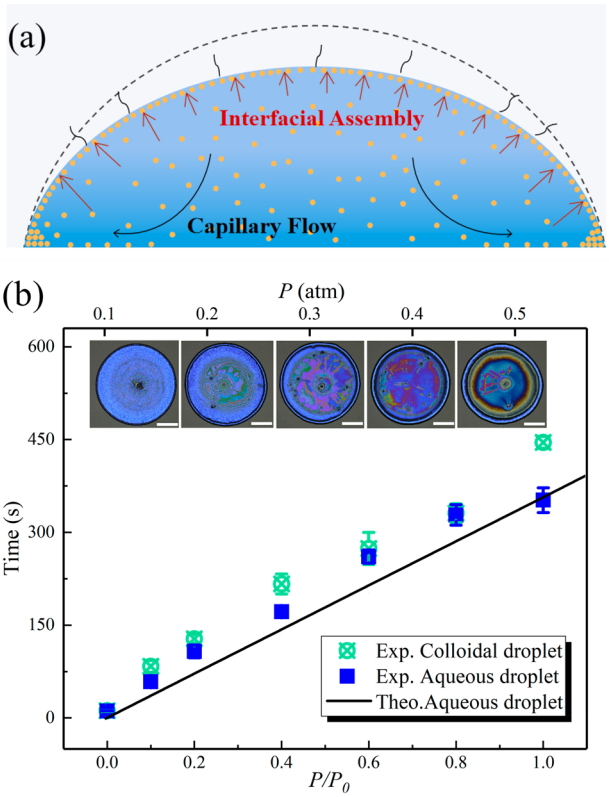

Figure 1. (a) Schematic diagram of the internal flow of droplets by the LPAE. The descent of the gas−liquid interface caused by rapid evaporation makes most of the particles to be captured by the interface and finally form ordered colloidal crystals. The capillary flow caused by uneven evaporation causes the particles to move to the edge and form a coffee ring. The comparison of the two flows affects the final deposition pattern. (b) Experimental values of evaporation time of colloidal droplets and experimental and theoretical values of aqueous droplet evaporation time under different pressures. The experimental results are consistent with the theoretical values, which indicates that the evaporation time of droplets is proportional to the pressure. The illustrations show the deposition patterns of colloidal droplets with a particle size of 193 nm, a volume of about 0.4 μL, and a concentration of 2 wt % at pressures of 0.1, 0.2, 0.3, 0.4, and 0.5 atm. The scale is 400 μm. It can be seen that, with the decrease of the pressure, the coffee ring gradually disappears and the colloidal crystals become more uniform and ordered. When the pressure is 0.1 atm, there is almost no coffee ring.

in Figure 1b represent the experimental results, in which the green points represent colloidal droplets and the blue points represent the aqueous droplets. As seen from Figure 1b, the experiment is in good agreement with the theory for aqueous droplets. However, the evaporation rate is slightly slower for colloidal droplets. Maybe it is due to the colloidal particles being captured and covering the gas−liquid interface, which reduces the effective evaporating area of the droplet, thus slowing the evaporation rate.

Therefore, we assume that the acceleration of the evaporation rate caused by a lower pressure could influence the interface capture effect, whose strength can be reflected by the Peclet number.[34−36] We estimate the Peclet number of the system

https://doi.org/10.1021/acs.jpclett.2c00534
J. Phys. Chem. Lett. 2022, 13, 3776−3780

$$Pe = \frac{h^2/D_L}{h/V_{ev}} \tag{8}$$

where $h = R\left(\frac{1}{\sin(\theta)} - \frac{1}{\tan(\theta)}\right)$ is the droplet height and V_{ev} is the speed at which the top surface moves downward

$$V_{ev} = \frac{\dot{m}}{\rho A} = \frac{\dot{m}}{\rho 2\pi h \frac{R}{\sin\theta}} \tag{9}$$

D_L is the diffusion coefficient

$$D_L = \frac{K_B T}{6\pi r \eta} \tag{10}$$

where $K_B = 1.38 \times 10^{-23}$ J/K is the Boltzmann constant, $r \approx 100$ nm is the particle radius, $\eta \approx 10^{-3}$ Pas is the viscosity coefficient of water, and A is the evaporation area of the droplet. When these parameter values are brought into equations, we finally obtain

$$Pe \approx 126\frac{P_0}{P} \propto \frac{1}{P} \tag{11}$$

It can be found that, when it is atmospheric pressure evaporation, $Pe \approx 126 \gg 1$. This means that the interface capture effect cannot be ignored in this system. With the decrease of the pressure, through eq 11, the Peclet number will further increase (for example, when $P = 0.1$ atm, $Pe \approx 1260$). In other words, the lower the pressure, the stronger the capture effect. Meanwhile, because the contact line is pinned and the contact angle is small, the capillary flow cannot be ignored either. Therefore, the final deposition pattern in this system might be determined by the competitive relationship between these two effects, as shown in Figure 1a. When the capillary flow caused by uneven evaporation dominates, most particles are transported to the edge of the droplet and form the coffee ring. When the pressure decreases, the interface capture effect gradually increases, and then most particles are captured by the interface; therefore, the coffee ring weakens.

We confirmed the above analysis through experiments. As shown in Figure 1b, with the decrease of the pressure, the Peclet number gradually increased and the coffee ring gradually weakened. In addition, we also noticed that, with the decrease of the pressure, the deposition pattern gradually became more uniform and the color became more bright. This means that an ordered crystal structure may be formed. By observation of the microstructure of the deposition pattern, a hexagonal close-packed (HCP) colloidal crystal can be obtained, as shown in Figure S2 of the Supporting Information. Therefore, the decrease of the pressure can not only improve the evaporation efficiency but also weaken the coffee ring and form a uniform and ordered structure.

For a further understanding of the assembly process of colloidal particles, the dynamic evolution of a flash evaporating droplet was *in situ* microscopically observed and studied. Figure 2 shows the color change during the whole evaporation process of a colloidal droplet under low-pressure conditions. The surface of the droplet rapidly appears light dark red after entering the low-pressure environment for 0.2 s, as shown in panels a and b of Figure 2. In the next 1 s, the color becomes brighter and brighter and becomes green near the edge, as shown in panels c and d of Figure 2. As evaporation progresses, in 1.74 s, the whole gas−liquid interface forms a dense arrangement, as shown in Figure 2e. After 2 s, the droplet color

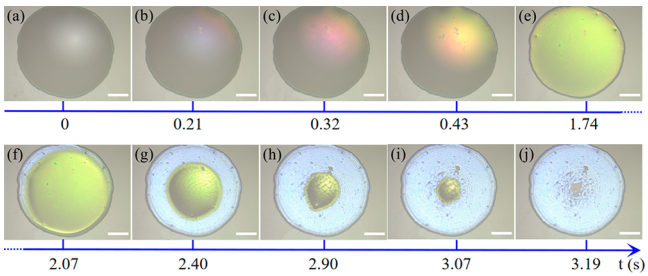

Figure 2. Droplet color change during the LPAE with a concentration of 1 wt % and a particle size of 193 nm at the pressure of 0.001 atm. (a and b) Color of the droplet surface changes rapidly after entering the low-pressure environment. (c and d) Change of color is more and more obvious, and the droplet edge reaches green faster than the middle. (e) Whole gas−liquid interface turns green. (f and g) As the droplet gradually evaporates, the edges begin to dewet and the color changes from green to blue. (h and i) Uniform particle layer on the liquid surface is gradually pulled and divided at last, resulting in fragmentation. (j) Particle layer on the liquid surface eventually spreads out onto the substrate in a fragmented state and even forms a hole.[37] The scale is 400 μm.

changes again as the contact line shrinks, as shown in panels f−j of Figure 2. We think that the color change of the droplet is caused by the film formed at the interface. Therefore, in the evaporation process, we conducted a disturbance test on the surface of the droplet (to disturb the interface during evaporation with a fine wire, and the fine wire was placed on the droplet surface in advance), confirming the existence of the film, as shown in panels a−f of Figure S3 of the Supporting Information. In addition, by replacement of large particles, the process of the island particle layer gradually forming at the interface is observed directly, as shown in Figure S3g of the Supporting Information.

To further verify the source of bright colors of the film formed on the surface, we measured the real-time reflection spectrum during evaporation. Then, we found that the film was a crystal structure (as shown in Figure S4 of the Supporting Information, the Bragg scattering peaks shift and increase with evaporation, corresponding to the gradual change and enhancement of color in Figure 2). As for the color of droplets changed from green to blue, this may be due to the ordered crystal film being transferred to the substrate. With the dewetting by the way of the contact line shrinking, the medium between particles changed from water to air, and then the color changed. By measurement of the change of scattering peaks after rewatering the pattern, the conjecture has been confirmed (as shown in Figure S5 of the Supporting Information).

Therefore, in the process of rapid evaporation caused by a low pressure, the capture effect of the gas−liquid interface is dominated. A large number of colloid particles are gradually captured by the gas−liquid interface, which will form an ordered crystal film structure immediately. With dewetting, the crystal film is transferred to the substrate, forming the final deposition pattern.

On the basis of the LPAE method, we realized the construction of multi-color photonic crystals by changing the particle diameter at an appropriate concentration. It is worth noting that the concentration will not only affect the uniformity of the pattern, but also as the concentration decreases, when the layer thickness is only several nanospheres, the color hues will change significantly[38] (for more detailed information about the effect of the concentration, see Figure

https://doi.org/10.1021/acs.jpclett.2c00534
J. Phys. Chem. Lett. 2022, 13, 3776−3780

S6 and part 6 of the Supporting Information). Here, we selected the particles with sizes of 193, 220, 240, and 310 nm, and the prepared photonic crystals correspond to blue, green, orange, and orchid in the illustration of Figure 3 [using

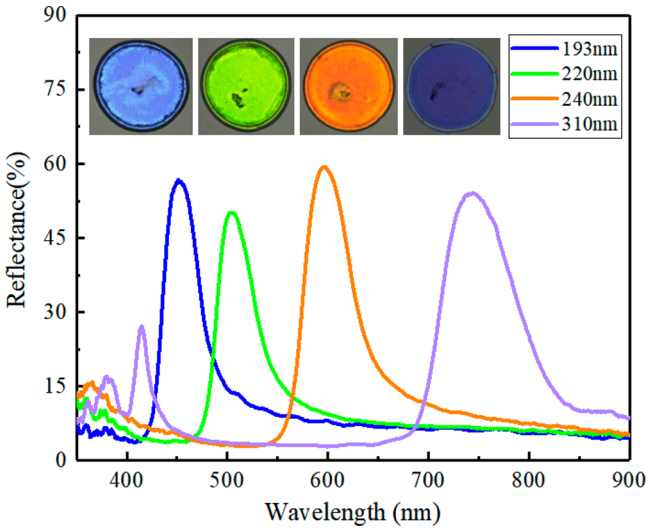

Figure 3. Deposition patterns and reflectance of colloidal solutions with different particle sizes. The concentration is 3 wt %, and the evaporation pressure is 0.2 atm. The diameters of particles are 193, 220, 250, and 310 nm. The four deposition patterns have beautiful colors, and the measurement of reflectivity by the spectrometer also proves that the photonic crystals deposited by the LPAE have high quality.

scanning electron microscopy (SEM), we observed the microstructure of the two kinds of particles, and they showed a HCP crystal structure, as shown in Figure S2 of the Supporting Information]. Through the measurement of the reflection spectrum, it can be found that the corresponding Bragg scattering wavelengths are consistent with the corresponding theoretical value (see part 7 of the Supporting Information for details). In comparison to the previous study, the LPAE method can realize the ultrafast construction of photonic crystals with rich and ordered structural colors. It is worth noting that we found that the LPAE process of droplets is insensitive to size to a certain extent. However, when the contact angle is too large or the heat transfer from the substrate is insufficient, freezing is likely to occur (see Figure S2 and part 8 of the Supporting Information for details).

In summary, we experimented with LPAE of colloidal droplets and found that the low-pressure environment can drastically increase the evaporation rate. Further analysis indicates that the increase of the evaporation rate will lead to the increase of the Peclet number and then strengthen the interface capture effect. Therefore, when the pressure decreases, a large number of particles will be quickly captured by the interface, thereby weakening the coffee ring effect. Through experiments and analysis, it is found that the particles captured by the interface will form an ordered crystal structure and finally be transported to the substrate. In the end, high-quality photonic crystals with diverse structural colors can be prepared ultrafast under flash evaporation by controlling several key factors, such as the pressure, concentration, and particle size. Through the LPAE method, the formation time of colloidal crystals can be shortened from hundreds of seconds under normal pressure to several seconds. We think that this method has potential applications for the high-efficient fabrication of large-area photonic crystals, perovskite solar cells, and printed flexible electronics.

■ ASSOCIATED CONTENT

Supporting Information

The Supporting Information is available free of charge at https://pubs.acs.org/doi/10.1021/acs.jpclett.2c00534.

Methodology, materials, and equipment (Figure S1), microstructural observations (Figure S2), *in situ* observation of the interfacial capture effect (Figure S3), dynamic spectral analysis of the gas−liquid interface (Figure S4), dynamic spectral analysis during rewetting of the dry pattern (Figure S5), effect of the initial concentrations on the deposition patterns (Figure S6), calculation of the Bragg scattering peak, and evaporation of different volumes (Figure S7) (PDF)

■ AUTHOR INFORMATION

Corresponding Authors

Weibin Li − *National Microgravity Laboratory, Institute of Mechanics, Chinese Academy of Sciences, Beijing 100190, People's Republic of China; School of Engineering Science, University of Chinese Academy of Sciences, Beijing 100049, People's Republic of China;* orcid.org/0000-0002-6406-1553; Email: liweibin@imech.ac.cn

Yuren Wang − *National Microgravity Laboratory, Institute of Mechanics, Chinese Academy of Sciences, Beijing 100190, People's Republic of China; School of Engineering Science, University of Chinese Academy of Sciences, Beijing 100049, People's Republic of China*; Email: yurenwang@imech.ac.cn

Author

Chen Zhang − *National Microgravity Laboratory, Institute of Mechanics, Chinese Academy of Sciences, Beijing 100190, People's Republic of China; School of Engineering Science, University of Chinese Academy of Sciences, Beijing 100049, People's Republic of China;* orcid.org/0000-0002-3947-492X

Complete contact information is available at: https://pubs.acs.org/10.1021/acs.jpclett.2c00534

Notes

The authors declare no competing financial interest.

■ ACKNOWLEDGMENTS

The authors gratefully acknowledge financial support from the National Natural Science Foundation of China (Grant 11902321).

■ REFERENCES

(1) Koshkina, O.; Raju, L. T.; Kaltbeitzel, A.; Riedinger, A.; Lohse, D.; Zhang, X.; Landfester, K. Surface Properties of Colloidal Particles Affect Colloidal Self-Assembly in Evaporating Self-Lubricating Ternary Droplets. *ACS Appl. Mater. Interfaces* **2022**, *14* (1), 2275−2290.

(2) Perkins-Howard, B.; Walker, A. R.; Do, Q.; Senadheera, D. I.; Hazzazi, F.; Grundhoefer, J. P.; Daniels-Race, T.; Garno, J. C. Surface Wettability Drives the Crystalline Surface Assembly of Monodisperse Spheres in Evaporative Colloidal Lithography. *J. Phys. Chem. C* **2022**, *126* (1), 505−516.

(3) Zolotarev, P. A.; Kolegov, K. S. Monte Carlo Simulation of Particle Size Separation in Evaporating Bi-dispersed Colloidal

Droplets on Hydrophilic Substrates. *Phys. Fluids* **2022**, *34* (1), 017107.
(4) Li, X.; Bi, D.; Yi, C.; Décoppet, J.-D.; Luo, J.; Zakeeruddin, S. M.; Hagfeldt, A.; Grätzel, M. A Vacuum Flash-Assisted Solution Process for High-Efficiency Large-Area Perovskite Solar Cells. *Science* **2016**, *353* (6294), 58−62.
(5) Yu, Y.; Yang, D.; Li, J.; Zhang, M.; Luo, H.; Liang, Q.; Ye, H.; Zhang, Q.; Tang, X.; Wu, J. A Flash Vacuum-Induced Reaction in Preparing High Performance Thermoelectric Cu2S. *Adv. Funct. Mater.* **2022**, *32* (2), 2107284.
(6) Grusser, M.; Waugh, D. G.; Lawrence, J.; Langer, N.; Scholz, D. On the Droplet Size and Application of Wettability Analysis for the Development of Ink and Printing Substrates. *Langmuir* **2019**, *35* (38), 12356−12365.
(7) Kolegov, K. S.; Barash, L. Y. Applying Droplets and Films in Evaporative Lithography. *Adv. Colloid Interface Sci.* **2020**, *285*, 102271.
(8) Smith, F. R.; Brutin, D. Wetting and Spreading of Human Blood: Recent Advances and Applications. *Curr. Opin. Colloid Interface Sci.* **2018**, *36*, 78−83.
(9) Chen, Y.; Min, X.; Zhang, X.; Zhang, F.; Lu, S.; Xu, L. P.; Lou, X.; Xia, F.; Zhang, X.; Wang, S. AIE-Based Superwettable Microchips for Evaporation and Aggregation Induced Fluorescence Enhancement Biosensing. *Biosens. Bioelectron.* **2018**, *111*, 124−130.
(10) Goh, G. L.; Saengchairat, N.; Agarwala, S.; Yeong, W. Y.; Tran, T. Sessile Droplets Containing Carbon Nanotubes: A Study of Evaporation Dynamics and CNT Alignment for Printed Electronics. *Nanoscale* **2019**, *11* (22), 10603−10614.
(11) Mao, Y.; Wu, Y.; Zhang, P.; Yu, Y.; He, Z.; Wang, Q. Nanocellulose-Based Reusable Liquid Metal Printed Electronics Fabricated by Evaporation-Induced Transfer Printing. *J. Mater. Sci. Technol.* **2021**, *61*, 132−137.
(12) Mampallil, D.; Eral, H. B. A Review on Suppression and Utilization of the Coffee-Ring Effect. *Adv. Colloid Interface Sci.* **2018**, *252*, 38−54.
(13) Lee, J.; Li, X.; Park, J. Suppression of Capillary Flow in Slot-Die Coating for the Fabrication of Fine OLED Stripe. *IEEE Trans. Electron Devices* **2019**, *66* (12), 5221−5229.
(14) Jung, K. I.; Park, B. S.; Lee, S. J.; Noh, S. M.; Jung, H. W. Effect of Immiscible Secondary Fluid on Particle Dynamics and Coffee Ring Characteristics during Suspension Drying. *Materials (Basel)* **2020**, *13* (15), 3438.
(15) Tian, Y.; Zhu, Z.; Li, Q.; Zhang, J.; Wang, C.-F.; Wu, G.; Li, S. S.; Xiao, J. J.; Chen, S. Rapid Visualized Hydrophobic-Force-Driving Self-Assembly towards Brilliant Photonic Crystals. *Chem. Eng. J.* **2021**, *420*, 127582.
(16) Deegan, R. D.; Bakajin, O.; Dupont, T. F.; Huber, G.; Nagel, S. R.; Witten, T. A. Capillary Flow as the Cause of Ring Stains from Dried Liquid Drops. *Nature* **1997**, *389* (6653), 827−829.
(17) Marin, A. G.; Gelderblom, H.; Lohse, D.; Snoeijer, J. H. Order-to-Disorder Transition in Ring-Shaped Colloidal Stains. *Phys. Rev. Lett.* **2011**, *107* (8), 085502.
(18) Hu, H.; Larson, R. G. Analysis of the Effects of Marangoni Stresses on the Microflow in An Evaporating Sessile Droplet. *Langmuir* **2005**, *21* (9), 3972−80.
(19) Hu, H.; Larson, R. G. Marangoni Effect Reverses Coffee-Ring Depositions. *J. Phys. Chem. B* **2006**, *110* (14), 7090−7094.
(20) Malinowski, R.; Volpe, G.; Parkin, I. P.; Volpe, G. Dynamic Control of Particle Deposition in Evaporating Droplets by an External Point Source of Vapor. *J. Phys. Chem. Lett.* **2018**, *9* (3), 659−664.
(21) Bhardwaj, R.; Fang, X.; Somasundaran, P.; Attinger, D. Self-Assembly of Colloidal Particles from Evaporating Droplets: Role of DLVO Interactions and Proposition of A Phase Diagram. *Langmuir* **2010**, *26* (11), 7833−7842.
(22) Lama, H.; Basavaraj, M. G.; Satapathy, D. K. Tailoring Crack Morphology in Coffee-Ring Deposits Via Substrate Heating. *Soft Matter* **2017**, *13* (32), 5445−5452.
(23) Edwards, A. M. J.; Atkinson, P. S.; Cheung, C. S.; Liang, H.; Fairhurst, D. J.; Ouali, F. F. Density-Driven Flows in Evaporating Binary Liquid Droplets. *Phys. Rev. Lett.* **2018**, *121* (18), 184501.
(24) Kim, J. Y.; Gonçalves, M.; Jung, N.; Kim, H.; Weon, B. M. Evaporation and Deposition of Inclined Colloidal Droplets. *Sci. Rep.* **2021**, *11* (1), 17784.
(25) Hu, G.; Yang, L.; Yang, Z.; Wang, Y.; Jin, X.; Dai, J.; Wu, Q.; Liu, S.; Zhu, X.; Wang, X.; Wu, T.-C.; Howe, R. C. T.; Albrow-Owen, T.; Ng, L. W. T.; Yang, Q.; Occhipinti, L. G.; Woodward, R. I.; Kelleher, E. J. R.; Sun, Z.; Huang, X.; Zhang, M.; Bain, C. D.; Hasan, T. A General Ink Formulation of 2D Crystals for Wafer-Scale Inkjet Printing. *Sci. Adv.* **2020**, *6* (33), No. eaba5029.
(26) Cui, L.; Zhang, X.; Wang, J.; Jiang, L. Functional Colloidal Assemblies Based on Superwettable Substrates. *Part. Part. Syst. Charact.* **2022**, *39* (1), 2100196.
(27) Zaibudeen, A. W.; Bandyopadhyay, R. DC Field Coupled Evaporation of A Sessile Gold Nanofluid Droplet. *Soft Matter* **2021**, *17* (45), 10294−10300.
(28) Yunker, P. J.; Still, T.; Lohr, M. A.; Yodh, A. G. Suppression of the Coffee-Ring Effect by Shape-Dependent Capillary Interactions. *Nature* **2011**, *476* (7360), 308−11.
(29) Li, W.; Ji, W.; Lan, D.; Wang, Y. Self-Assembly of Ordered Microparticle Monolayers from Drying a Droplet on a Liquid Substrate. *J. Phys. Chem. Lett.* **2019**, *10* (20), 6184−6188.
(30) Li, Y.; Yang, Q.; Li, M.; Song, Y. Rate-Dependent Interface Capture Beyond the Coffee-Ring Effect. *Sci. Rep.* **2016**, *6* (1), 24628.
(31) Chatterjee, S.; Kumar, M.; Murallidharan, J. S.; Bhardwaj, R. Evaporation of Initially Heated Sessile Droplets and the Resultant Dried Colloidal Deposits on Substrates Held at Ambient Temperature. *Langmuir* **2020**, *36* (29), 8407−8421.
(32) Hu, H.; Larson, R. G. Evaporation of a Sessile Droplet on a Substrate. *J. Phys. Chem. B* **2002**, *106* (6), 1334−1344.
(33) Sobac, B.; Brutin, D. Thermal Effects of the Substrate on Water Droplet Evaporation. *Phys. Rev. E* **2012**, *86* (2), 021602.
(34) Fortini, A.; Martin-Fabiani, I.; De La Haye, J. L.; Dugas, P.-Y.; Lansalot, M.; D'Agosto, F.; Bourgeat-Lami, E.; Keddie, J. L.; Sear, R. P. Dynamic Stratification in Drying Films of Colloidal Mixtures. *Phys. Rev. Lett.* **2016**, *116* (11), 118301.
(35) Liu, W.; Midya, J.; Kappl, M.; Butt, H.; Nikoubashman, A. Segregation in Drying Binary Colloidal Droplets. *ACS Nano* **2019**, *13*, 4972−4979.
(36) Thayyil Raju, L.; Koshkina, O.; Tan, H.; Riedinger, A.; Landfester, K.; Lohse, D.; Zhang, X. Particle Size Determines the Shape of Supraparticles in Self-Lubricating Ternary Droplets. *ACS Nano* **2021**, *15* (3), 4256−4267.
(37) Man, X.; Doi, M. Ring to Mountain Transition in Deposition Pattern of Drying Droplets. *Phys. Rev. Lett.* **2016**, *116* (6), 066101.
(38) Yuan, W.; Li, Q.; Zhou, N.; Zhang, S.; Ding, C.; Shi, L.; Zhang, K.-Q. Structural Color Fibers Directly Drawn from Colloidal Suspensions with Controllable Optical Properties. *ACS Appl. Mater. Interfaces* **2019**, *11* (21), 19388−19396.

https://doi.org/10.1021/acs.jpclett.2c00534
J. Phys. Chem. Lett. 2022, 13, 3776−3780